Chemical Engineering Science 117 (2014) 248–263

Contents lists available at ScienceDirect

Chemical Engineering Science

journal homepage: www.elsevier.com/locate/ces

Experimental investigation of hysteresis in the break-up of liquid curtains

J.O. Marston [a,*], S.T. Thoroddsen [a], J. Thompson [b], M.G. Blyth [b], D. Henry [c], J. Uddin [c]

[a] Division of Physical Sciences and Engineering, King Abdullah University of Science and Technology, Thuwal 23955-6900, Saudi Arabia
[b] School of Mathematics, University of East Anglia, Norwich NR4 7TJ, UK
[c] School of Mathematics, University of Birmingham, Edgbaston B15 2TT, UK

HIGHLIGHTS

- We investigate the break-up of multi-layer liquid curtains experimentally.
- Hysteresis windows are identified for both single-layer and multi-layer curtains.
- The origins of break-up are assessed with high-speed video imaging.
- The post-break-up thread formation is analysed and compared to previous studies.

ARTICLE INFO

Article history:
Received 14 November 2013
Received in revised form
15 May 2014
Accepted 18 June 2014
Available online 2 July 2014

Keywords:
Liquid curtain
Taylor-Culick
Rupture
Rayleigh-Taylor

ABSTRACT

Findings from an experimental investigation of the break-up of liquid curtains are reported, with the overall aim of examining stability windows for multi-layer liquid curtains composed of Newtonian fluids, where the properties of each layer can be kept constant or varied. For a single-layer curtain it is known that the minimum flow rate required for initial stability can be violated by carefully reducing the flow rate below this point, which defines a hysteresis region. However, when two or three layers are used to form a composite curtain, the hysteresis window can be considerably reduced depending on the experimental procedure used. Extensive quantitative measurements of this hysteresis region are provided alongside an examination of the influence of physical properties such as viscosity and surface tension. The origins of curtain break-up for two different geometries are analysed; first where the curtain width remains constant, pinned by straight edge guides; and second where the curtain is tapered by angled edge guides. For both cases, the rupture speed is measured, which appears to be consistent with the Taylor–Culick velocity. Observations of the typical linearly spaced jets which form after the break-up has transpired and the periodicity of these jets are compared to the Rayleigh–Taylor wavelength and previous experimental measurements. Furthermore, the curtain stability criterion originally developed by Brown (1961), summarised in terms of a Weber number, has recently been extended to multi-layer curtains by Dyson et al. (2009); thus this report provides the first experimental measurements which puts this to the test. Ultimately, it is found that only the most viscous and polymer-based liquids violate this criterion.

1. Introduction

1.1. Curtain stability

The break-up of a liquid curtain is a phenomenon that has fascinated scholars of fluid mechanics since Taylor's work on the disintegration of liquid sheets in 1959. Subsequent interest in this particular field may have evolved, in part, from the practical application of liquid curtains in the coating industry, namely the method known as "curtain coating" whereby a thin liquid curtain falls vertically to impinge upon a moving substrate that can travel at high-speed underneath the curtain without entraining air bubbles (e.g. Blake et al., 1994, 2004; Marston et al., 2006, 2007)

Brown (1961) made progress on Taylor's original work by performing a simple stability analysis which ultimately resulted in a balance between inertia and surface tension in the curtain. His analysis concluded that to maintain curtain stability, the following Weber number criterion must be satisfied:

$$We = \frac{\rho Q v_c}{2\sigma} > 1, \tag{1}$$

* Corresponding author. Current address: Department of Chemical Engineering, Texas Tech University, Lubbock, TX 79409-3121, USA.
E-mail address: jeremyom@hotmail.com (J.O. Marston).

http://dx.doi.org/10.1016/j.ces.2014.06.030
0009-2509/

where ρ is the liquid density, Q is the flow rate per unit width of curtain, v_c is the vertical component of the local curtain velocity and σ is the dynamic surface tension.

Subsequent investigations into the dynamics of liquid sheets focused on verifying this criterion, e.g. Lin and Roberts (1981), Lin (1981) and Lin et al. (1990), who analysed the growth of both temporally and spatially varying disturbances to a viscous liquid curtain, but ultimately finding excellent agreement with Brown's prediction. Motivated, in part, by Brown's criterion and observations of Taylor (1959), Antoniades et al. (1980) proposed that the balance between inertia and surface tension could be exploited to determine the dynamic surface tension, σ_{dyn}, by placing an obstacle in the curtain such that a free edge forms at an angle, θ, from vertical, emanating from the obstacle, whereby $2\sigma_{dyn} = \rho Q v_c \sin^2\theta$.

In contrast to work supporting the original Weber number criterion of Brown (1961), Finnicum et al. (1993), De Luca (1999) and Roche et al. (2006) all showed experimentally that violations of the Weber number criterion are possible. Even Brown himself noted that curtains with $We < 1$ were possible if the location where $We = 1$ is in the vicinity of the slot. These observations thus indicate that the curtain can exhibit metastable or hysteresis regions with respect to the flow rate. It is noted, however, that these observations were all reported through experiments with slot-die configurations (see also the comprehensive works of Weinstein et al., 1997, Clarke et al., 1997 and Weinstein et al., 1998 for the governing equations of motion of curtains from such geometries). In some cases (e.g. Roche et al., 2006), it is possible that curtain ruptures can 'self-heal', which may be partly explained by the stabilising effect of viscosity (De Luca and Costa, 1997). However, as argued in Miyamoto and Katagiri (1997), the stabilising effect of viscosity may be limited due to the development of viscous boundary layers along the edge guides, which are employed to maintain the integrity of a falling liquid curtain (e.g. Schweizer and Troller, 2000; Schweizer and Krebs, 2003).

In contrast, there does not appear to be corresponding measurements for slide-die geometries, where the curtain emanates from the lip of a slide. In this case, both Lin and Krishna (1978) and Kistler and Scriven (1994) showed that deflection towards the underside of the slide can become significant and is influenced by both physical properties of the liquid and the velocity gradient, since the bottom side of the liquid is pinned at the lip compared to the top face of the curtain which is travelling faster. This effect is known as the "teapot effect", also discussed by Doell et al. (2009).

Fig. 1 provides schematic representations of both (a) slot and (b) slide die configurations for liquid curtains. In addition, Fig. 1 (c) shows the general configuration that is considered in the experimental work herein for multi-layer flows.

Generalising the original Weber number criterion of Brown (1961) has been the focus of some recent work; motivated by advances in coating technology and the advent of multi-layer coatings, which can involve over 10 layers of fluid, Dyson et al. (2009) derived the equivalent stability criterion for a liquid curtain composed of n layers:

$$\frac{v_c \sum_{j=1}^{n} \rho_j Q_j}{\sum_{j=0}^{n} \sigma_j} > 1, \tag{2}$$

where σ_0 represents the surface tension of the liquid–gas interface of the first (bottom) layer, σ_1 the interfacial tension between layers 1 and 2 and so on. This criterion has yet to be tested experimentally.

Despite the numerous studies, both theoretical and experimental, surrounding the stability of falling liquid curtains, it is clear that the hysteresis in terms of flow rate required for stability needs to be addressed in detail, specifically for slide-die geometries as this was not considered in the previous studies which observed this effect. It is also evident that no previous experimental studies exist for the break-up of liquid curtains formed from multiple layers of fluid, despite the clear relevance to multi-layer coating. The generalised criterion (Eq. (2)) proposed by Dyson et al. (2009) also needs to be subjected to experimental validation. This is a primary motivation of the present experimental study.

1.2. Curtain break-up

If a liquid curtain becomes unstable and ruptures, multiple different flow regimes can be observed. One of the most compelling studies to highlight this observation was by Pritchard (1986) who reported over seven hundred different flow regimes for a layer of oil flowing over the end of a sharp plate, which exhibited both periodic and chaotic behavior. De Luca and Meola (1995) also carried out an extensive experimental investigation of the break-up of a sheet exiting from various nozzle geometries in a slot-die configuration. Their work also reported multiple different flow regimes and focused on the role of surfactants in the onset of instability, which is assumed to be due to the capillary rupture. In order to quantify their findings, they introduced a *surface pressure*, $\Pi = \sigma_s - \sigma$, where σ_s is the surface tension of the solvent and σ is that of the solution containing the surfactant. They found that the critical flow rate at the break-up of the curtain, Q_c, was a strong function of Π. In particular, when regularly spaced threads are formed as a result of rupture, they found a linear correlation between the momentum in the curtain evaluated at break-up, $\rho Q_{thr}^2/h_c$, and Π, where Q_{thr} is the flow rate when the threads are observed and $h_c \approx Q_{thr}/(2gz_c)^{1/2}$ is the local curtain thickness at break-up and z_c is the vertical distance from the exit slot to the origin of the break-up. They ultimately found that the spacing between the threads, typically between 1 and 4 cm, was an increasing function of surface tension and fitted their data to the following empirical equation:

$$\frac{s}{h_0} = 20We^{-0.52}, \tag{3}$$

where s is the spacing between threads and δ_0 is the exit slot width (i.e. the initial curtain width) and We is evaluated at rupture.

In related experiments, Limat et al. (1992), Giorgiutti et al. (1995), Brunet (2007) and Brunet et al. (2007) investigated the flow of a liquid over hollow cylinders and circular plates and reported both dripping and jetting regimes, respectively where the jetting regime appears qualitatively similar to the threads observed by De Luca and Meola (1995). See also Becerra and Carvalho (2011). It was found that the spatial periodicity of the jets (or threads) was independent of the flow rate and governed instead by the wavelength of the Rayleigh–Taylor instability whereby

$$\lambda_{threads} = 2\pi\sqrt{2\sigma/(\rho g)}. \tag{4}$$

This lengthscale is approximately 1–2 cm for most liquids used in experimental studies wherein $\rho \approx 1000\ \mathrm{kg\,m^{-3}}$ and $\sigma =$ 20–72 mN/m.

During the break-up of a falling liquid curtain, prior to the formation of threads, a hole essentially must open up that propagates far enough upstream to cause the entire sheet to rupture. Typically, the opening speed of a puncture in a liquid film can be given by the well-stablished Taylor–Culick speed

$$U_{open} = \sqrt{2\sigma/(\rho H)}, \tag{5}$$

which was investigated for viscous-dominated systems by Brenner and Gueyffier (1999) and Savva and Bush (2009), and more specifically in a falling curtain by Sunderhauf et al. (2002).

The secondary aim of this study is thus to examine both the rupture speed in a multi-layer falling liquid film *and* the formations after the break-up has transpired.

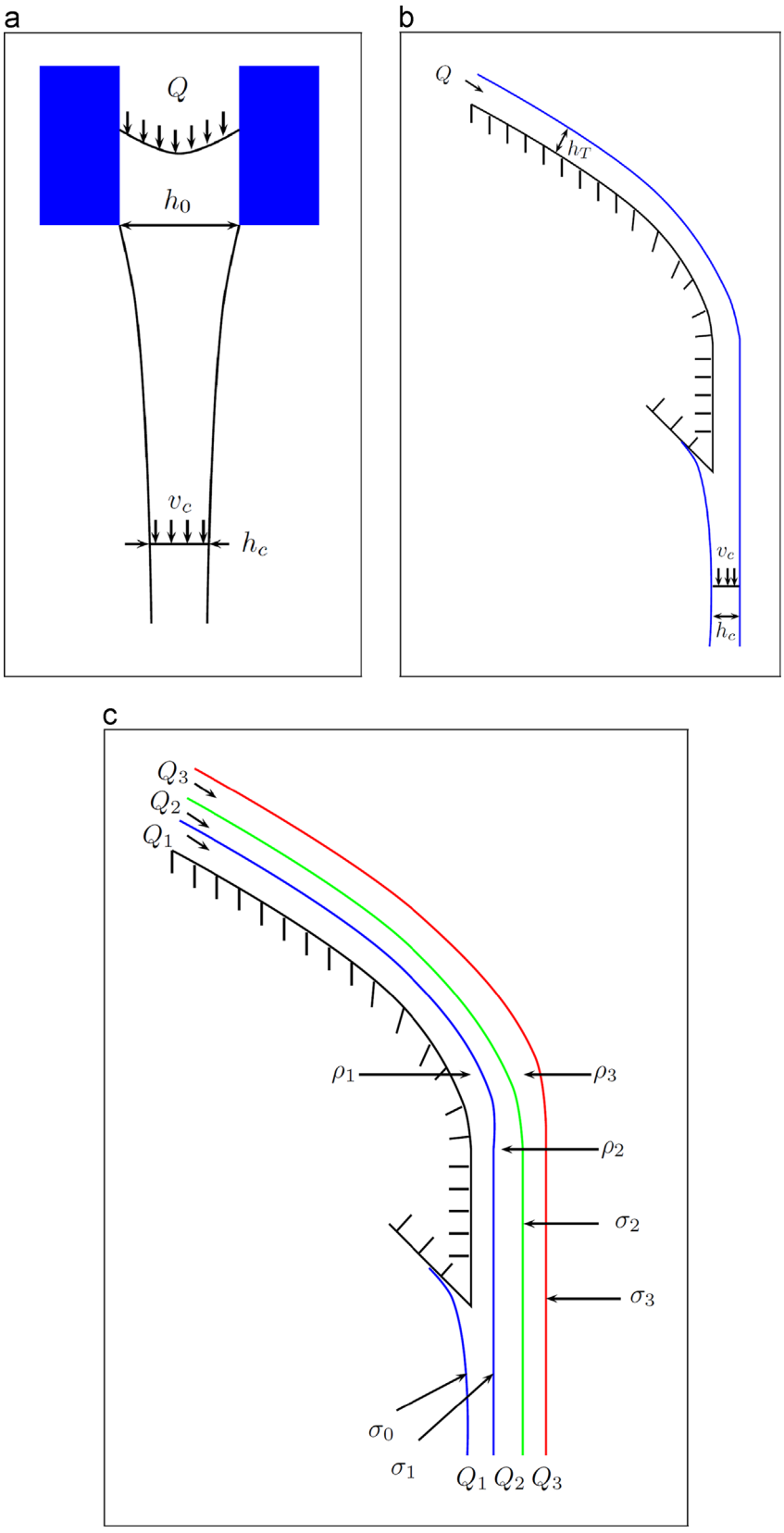

Fig. 1. Geometries of different configurations for curtain-forming flows: (a) 1-layer curtain from a slot-die, (b) 1-layer curtain from a slide-die, and (c) 3-layer curtain from a slide-die.

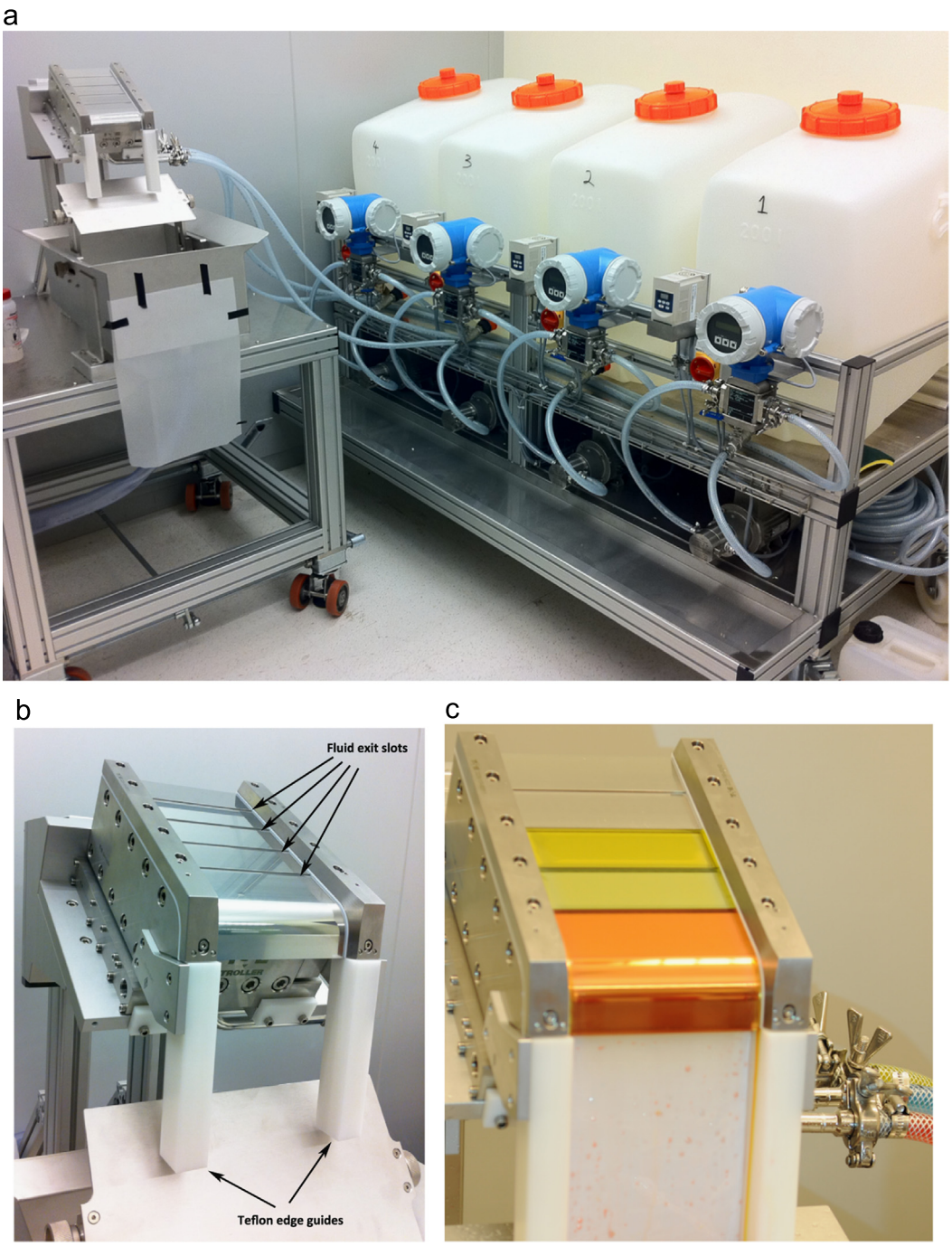

Fig. 2. Photographs of the experimental setup. (a) Photograph of the whole facility showing the "coating station" and the "pumping station"; (b) photograph of the 4-layer slide die with Teflon edge guides; (c) photograph of a stable 3-layer curtain where different food dyes have been added to the layers for visualisation purposes only. (For interpretation of the references to colour in this figure caption, the reader is referred to the web version of this paper.)

2. Experimental setup and methods

2.1. Mechanical components

The experiments were performed on a custom-design pilot-scale facility, shown in Fig. 2(a). The main component is a 4-layer stainless steel slide die (TSE Troller AG, Switzerland), which is 12 cm wide and mounted at 30° from horizontal onto an aluminium frame, above a stainless steel catch-pan which collects the fluid.

Fluid is pumped from holding tanks into the die cavities and exits through the slots on the top face of the die (Fig. 3(b)) with a laminar flow profile. The fluid easily wets the face of the die due to a patterned grinding finish, with a surface roughness of $R_a = 0.1$ μm ($R_{t,max} = 1.2$ μm). Each slot on the die face has an exit width of 500 μm. An example image of a stable 3-layer curtain is shown in Fig. 2(c), where food colouring has been added to aid visualisation of the individual layers on the die.

The gear pumps were able to deliver fluid flow rates from approximately 0.25 l/min up to 7 l/min and the exact flow rate was read from an electromagnetic flowmeter (Proline Promag series 50H, Switzerland). The flow rates for each individual layer are then converted to a flow rate per unit width of curtain, $0.3 \leq Q \leq 9.7$ cm^2 s^{-1}.

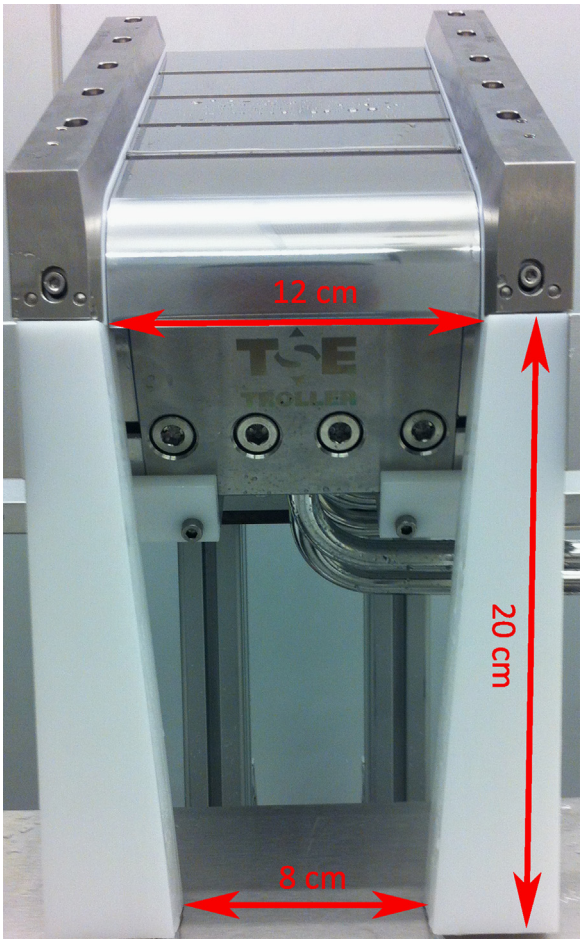

Fig. 3. Geometry used for the angled Teflon edge guides. The edge guides are 20 cm in length and the width of the edge guides at the base is 8 cm.

The curtain width is maintained using Teflon edge guides, shown in Fig. 2(b) and Fig. 3, which are mounted vertically at either side of the lip of the die.

2.2. Protocol for determining Q_{min} and Q_{thr}

In order to initially form a stable curtain for a given fluid, a minimum flow, Q_{min}, is required (e.g. Fig. 4(a)). To determine this flow rate, the flow to the die was started at a typically low flow rate, $Q \approx 0.5\ \mathrm{cm^2\ s^{-1}}$. The flow rate was then slowly increased until the curtain could either "pin" itself to the edge guides or by manually pinning using a thin plastic rod. This procedure was repeated several times in order to accurately determine Q_{min} and was found to be very repeatable (see later for more details). For consistency, the value of Q found by the manual pinning method is taken as Q_{min} in all cases.

Once a stable curtain was formed, the flow was left unchanged for at least one minute before the flow rate was slowly decreased. The flow rate was continuously, but slowly, decreased until break-up was observed with the naked eye. Typically, the break-up manifests itself in the form of vertical threads, such as those presented in Fig. 4(b). However, in order to assess the break-up in more detail, a high-speed camera (Photron Fastcam SA-3) operating at frame rates up to 1000 fps was employed. For each different configuration (i.e. for each fluid and for each different numbers of layers), a minimum of eight repeat measurements of Q_{thr} were taken to determine the break-up point. Note that once the break-up has occurred, the flow rate can be increased back to Q_{min} with several different possible configurations as shown in Fig. 4(c)–(f).

When performing 2-layer experiments, the flow rate of layer 1, Q_1, was first fixed, and then the above procedure was repeated for the flow rate in layer 2, Q_2. For a 3-layer experiment there are two cases; the first is where Q_1 and Q_2 are first fixed, and then the above procedure was repeated for Q_3; and the second case is where Q_1 and Q_2 are first fixed and Q_3 was adjusted to initially form a stable curtain, but then Q_2 was varied to observe break-up.

In some cases, experiments were repeated with angled edge guides shown in Fig. 3, which are known (e.g. Becerra and Carvalho, 2011) to increase curtain stability. In this case, the flow rate per unit width then becomes dependent on the fall height of the curtain according to the following equation:

$$Q(z) = \frac{Q_0}{1 - z/60}, \tag{6}$$

where $Q_0 = Q(z = 0)$. This correction is used in combination with the exact location of break-up from the high-speed video sequence in order to accurately determine the local Weber number at the point of break-up.

2.3. Fluid properties

The fluids used in the experiments were mostly water–glycerol mixtures, as shown in Table 1. In most cases, surfactant (CTAB or SDS) was added to the mixture to ensure that a curtain could be formed using the edge guides employed. The surface tension was characterised using a du Nouy ring or Wilhelmy plate tensiometer (K100 MK2/SF/C, Kruss GmbH, Germany), whilst viscosities were measured using a cone-and-plate geometry on a rotational rheometer (ARES-G2, TA Instruments, USA). In addition, solutions of polyvinyl alcohol (PVA) were also used, which have good wetting properties and thus do not require surfactant in order to form a curtain.

The surface tensions reported herein are essentially *static* or *equilibrium* values since they are measured using a method to determine such values in contrast to bubble pressure tensiometers, for example, where a dynamic surface tension can be measured. However, given the location of the break-ups observed (see Section 6), it is assumed that the free-surfaces (i.e. the rear face of the bottom layer and the front face of the top layer) are in equilibrium by the time (or height) at which rupture first occurs. This point is further discussed in Section 6. For a schematic representation of the assumed surfactant migration, see Fig. 5(a) and (b).

3. Description of flows on the die and in the curtain

3.1. Flow along the die

For an n-layer film flowing down an incline, the total volumetric flow rate that will ultimately be delivered to the curtain is the sum of the individual layers, i.e.

$$Q_T = \sum_{j=1}^{n} Q_j. \tag{7}$$

Along the face of the die, Weinstein (1990) and Jiang et al. (2005) have conducted extensive analyses for single and 3-layer flows down an inclined wall and the convention presented in Jiang et al. (2005) is adopted as follows: the total film thickness is denoted by h_T, which is used to scale distance, and is

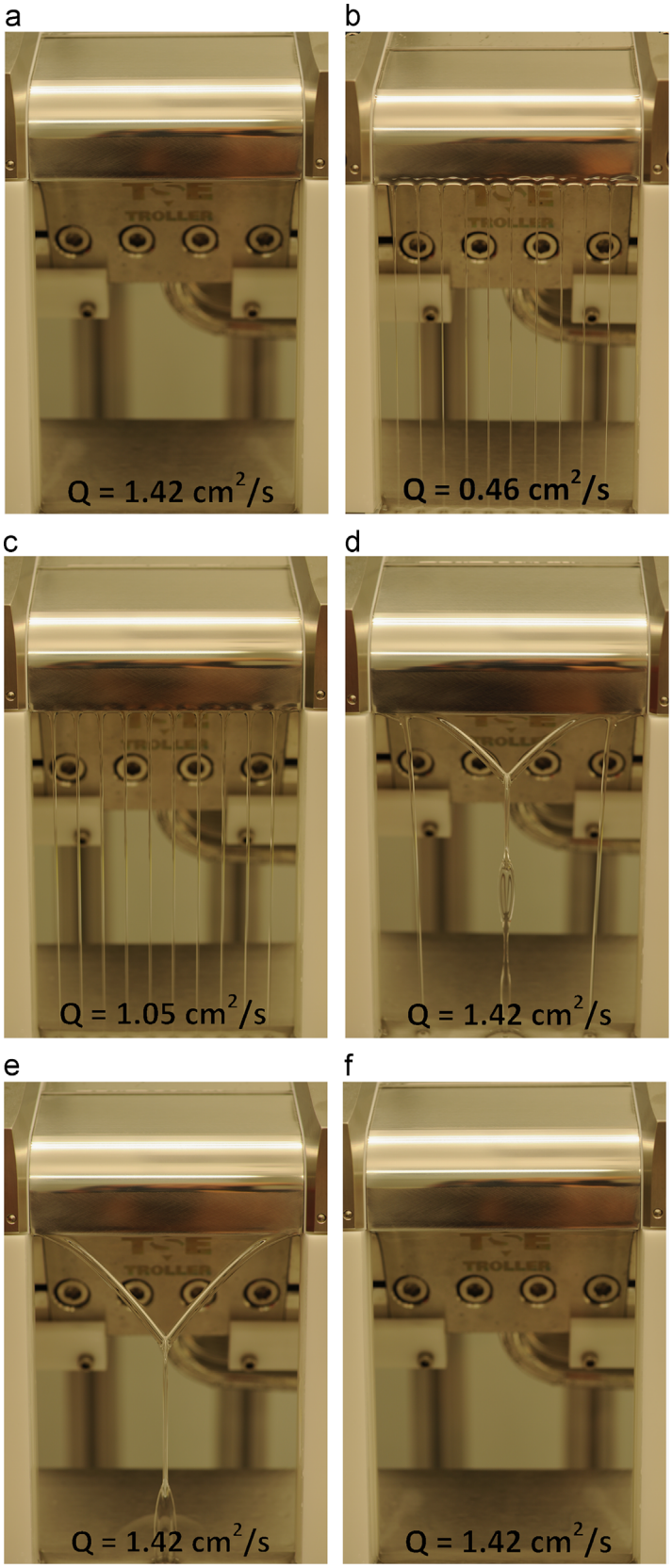

Fig. 4. Photographs of different formations observed by increasing and decreasing the liquid flow rate, Q (cm^2/s). Image (a) shows a stable liquid curtain, pinned at the edges by Teflon edge guides, while (b) shows the formation of threads momentarily after break-up. The flow rate increases slowly from (b)–(c)–(d). Images (d)–(f) show three different configurations for an identical flow rate.

approximated by

$$h_T = \left(\frac{3Q_T\mu_1}{\rho g \sin\theta}\right)^{1/3} \tag{8}$$

where $\theta = 30^\circ$ is the incline for our experimental setup and μ_1 is the dynamic viscosity of layer 1. Note ρ is the density of each layer, assuming that each layer has the same density (which is not always true for multi-layer films, hence $\rho \equiv \rho_1$). The velocity scale is based on the single-layer free-surface velocity, given by

$$U_s = \frac{\rho g h_T^2 \sin\theta}{2\mu_1}. \tag{9}$$

Table 1
Physical properties of the glycerol-based coating fluids used in the experiments. The stated values were measured at the ambient temperature of the laboratory during the experiments (21 °C).

Glycerol conc. (%$_{w/w}$)	Surfactant conc. (%$_{w/w}$)	Viscosity μ (mPa s)	Density ρ (kg/m^3)	Surface tension σ (mN/m)
65.5	0.01 CTAB	15.4	1171	50.8
65.5	0.023 CTAB	15.4	1171	47.9
74	0.05 SDS	33.4	1196	54.47
74	0.21 SDS	33.4	1196	42.21
83.5	0.21 SDS	70	1219	47.13
91.9	0.1 SDS	262	1241	59.5
91.9	0.21 SDS	262	1241	54.8
79.1	0.05 SDS	52.9	1207	58.3
79.1	0.1 SDS	52.9	1207	53.6
79.1	0.2 SDS	52.9	1207	43.7
91.9	–	262	1241	65.1
89.4	–	174	1235	66.4
86.9	–	123	1228	66.6
85.2	–	87	1224	67.2
9.1% PVA	–	32.6	1028	43.3

Using these definitions for h_T and U_s, the following dimensionless groups can be formed:

$$Re = \frac{3\rho Q_T}{2\mu_1}, \quad N_j = \frac{\mu_j}{\mu_1}, \quad H_j = \frac{h_j}{h_T}, \quad Ca = \frac{\mu_1 U_s}{\sigma_1}, \tag{10}$$

where σ_1 is the liquid–gas interfacial tension (surface tension) of layer 1.

3.2. Flow in the curtain

Once having left the die face, and assuming plug flow in all layers, the local curtain thickness is given by

$$h_c = Q_T/v_c. \tag{11}$$

The local curtain velocity, $v_c(z)$, was shown by several authors (e.g. Blake et al., 1994; Weinstein et al., 1997; Clarke et al., 1997) to be in accord with the free-fall approximation

$$v_c = (v_0 + 2gz)^{1/2} \tag{12}$$

where, for a slide-die configuration, v_0 is the velocity of the liquid as it departs from the lip of the slide die and z is the vertical distance travelled below the lip. Furthermore, for $z \geq 2$ cm, it was shown (Clarke et al., 1997) that the pure free-fall approximation suffices, that is $v_c \approx (2gz)^{1/2}$.

The Reynolds number in the curtain is then defined as

$$Re_c = \frac{\rho_1 Q_T}{\mu_1}. \tag{13}$$

The use of solid edge guides will result in the development of boundary layers in the vicinity of the edge guides, where the boundary layer thickness is estimated using the Blasius solution (e.g. Bird et al., 2007):

$$\delta \approx 4.91\sqrt{\frac{\mu z}{\rho v_c}}. \tag{14}$$

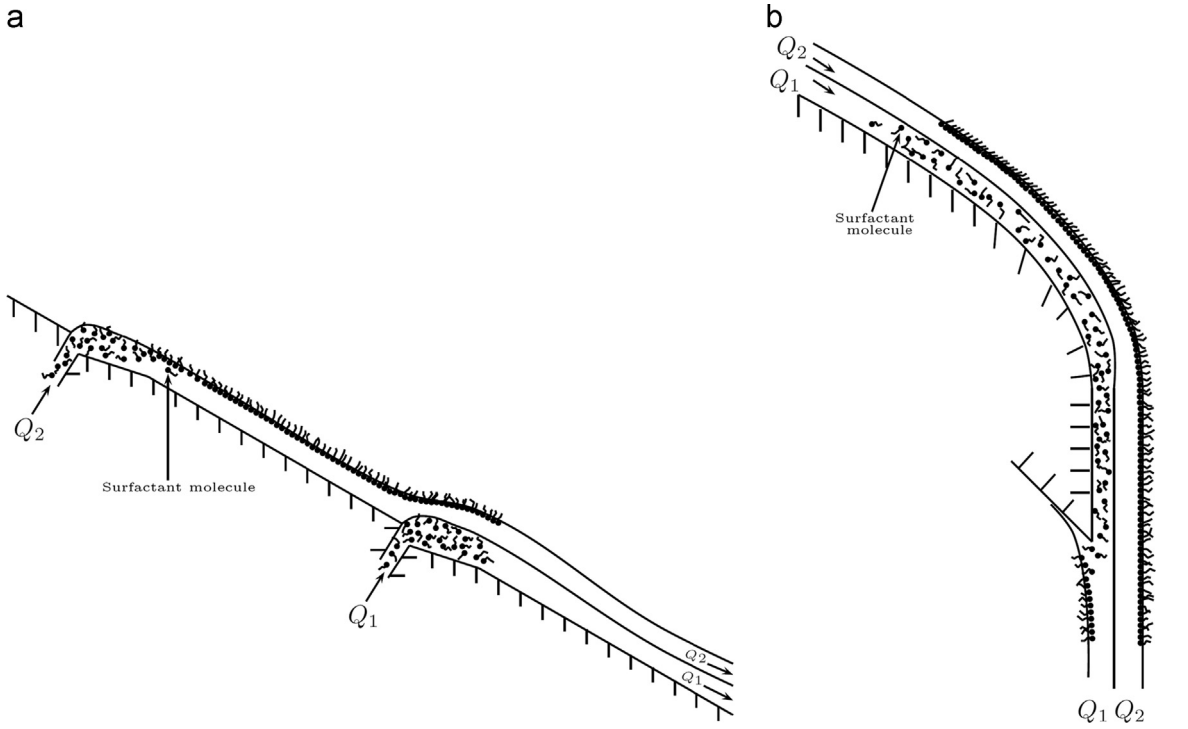

Fig. 5. Schematic representations of surfactant molecule migration (a) during flow down the die face and (b) near the lip or curtain-forming zone.

Close to the edge guide, the surface velocity can be estimated by substitution of Eq. (8) into (9) to yield

$$v_{edge} = \left(\frac{9\rho g \cos(\beta) Q^2}{8\mu}\right)^{1/3}, \quad (15)$$

where β is the inclination angle (from vertical) of the edge guides used. Eqs. (14) and (15) thus imply that typical edge effects extend 1–10 mm into the curtain with corresponding velocities $v_{edge} \sim$ 0.05–0.3 m/s.

Following Dyson et al. (2009), the Weber number in the curtain is then given by

$$We_T = \frac{v_c \sum_{j=1}^{n} \rho_j Q_j}{\sum_{j=0}^{n} \sigma_j}, \quad (16)$$

where σ_0 and σ_3 are the surface tensions of the bottom and top layers respectively. σ_1 and σ_2 (see Fig. 1(c)) will be taken as the absolute difference in surface tensions between the two layers, since the layers are mostly miscible and determining an exact interfacial tension becomes problematic.

4. Results: hysteresis

4.1. 1-layer curtain

In Fig. 6, an example of the hysteresis window is given in the *Re–We* parameter space for a nominal 60% glycerol mixture. The value of *We* was based on a local curtain velocity, $v_c = 1.5$ m/s, which was based upon the average vertical distance from the die lip to the initial break-up origin. In this plot, the solid blue data point represents the value of $Q_{min} = 1.8$ cm^2 s^{-1}, i.e. the minimum flow rate initially required to form a stable curtain. The red open square and the red star indicate the limits of the range of $Q_{thr} \in [0.64, 1.04]$ cm^2 s^{-1} observed over repeat trials. Thus the true hysteresis window is defined as $(\max(Q_{thr}), Q_{min}]$, indicated by the blue dashed line. This line therefore represents the region of metastability in this parameter space and it is precisely this region which is investigated in detail in the remainder of this section. Note also that the range of Weber number observed in Fig. 6 far exceeds those anticipated from the well-established stability criterion of Eq. (1). This is examined in detail in Section 6.

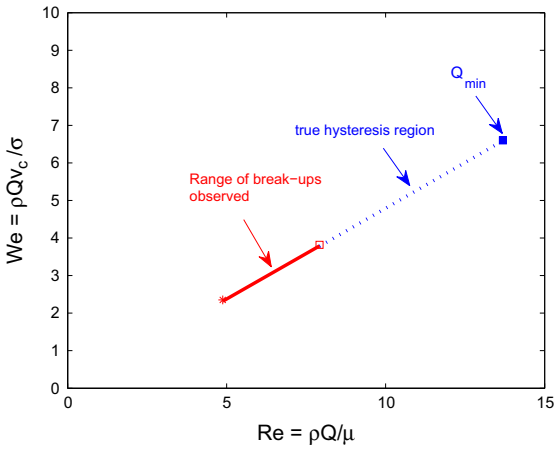

Fig. 6. Plot of the hysteresis region in the *Re–We* parameter space for a 1-layer 60% glycerol curtain ($\mu = 15.4$ mPa s, $\rho = 1171$ kg/m^3, $\sigma = 47.9$ mN/m). The Weber number is based on a local curtain velocity of $v_c = 1.5$ m/s, based upon the average initial disturbance location, $z_{break} = 10$ cm. (For interpretation of the references to colour in this figure caption, the reader is referred to the web version of this paper.)

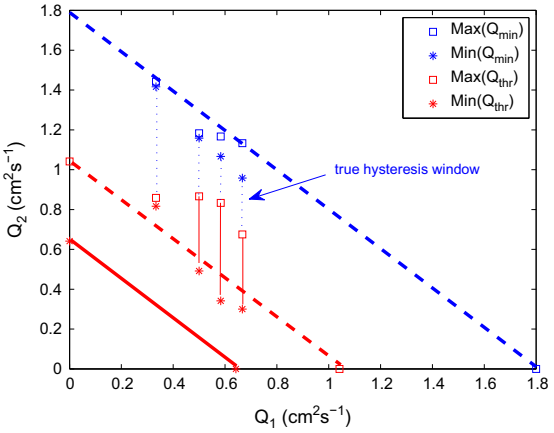

Fig. 7. Plot of Q_{min} and Q_{thr} for a 2-layer curtain where both layers are the same fluid ($\mu = 15.4$ mPa s, $\rho = 1171$ kg/m^3, $\sigma = 47.9$ mN/m). The diagonal dashed lines plot the "expected" limits of the hysteresis window based on the 1-layer experiments in Fig. 6. (For interpretation of the references to colour in this figure caption, the reader is referred to the web version of this paper.)

4.2. Multiple layers of the same fluid

Extending the results of Fig. 6 to a 2-layer curtain, shown in Fig. 7, one can see that the minimum flow rate required for curtain stability is generally lower for a 2-layer curtain than for the 1-layer curtain. This is evident from the data points (solid blue squares and blue stars) which all reside beneath the diagonal blue line, which represents the value $Q_T = Q_1 + Q_2 = 1.8$ cm^2 s^{-1}, based on the 1-layer experiment. In this 2-layer experiment, where the discrete layers are separated only by the differential motion between each other, a small range in Q_{min} is observed, which was not present for the 1-layer curtain. In this case, the true hysteresis window is defined as $(\max(Q_{thr}), \min(Q_{min})]$.

It is also apparent that the true hysteresis window becomes smaller, which again is evident from the data points for $\max(Q_{thr})$ (open red squares), which all lie above the dashed red line. Note also that none of the data points for $\min(Q_{thr})$ extend down to the solid red line, which represents the minimum value found for the break-up of the 1-layer curtain, $Q_{thr} = 0.64$ cm^2 s^{-1}.

Fig. 7 thus indicates that for a 2-layer curtain, $Q_{T,min} < Q_{min}$, but that $Q_{T,thr} > Q_{thr}$, where Q_{min} and Q_{thr} refer strictly to the 1-layer curtain. In other words, the hysteresis windows have been reduced. This observation may be due in part to the differential motion between layers, whereby the top layer is subject to free-slip at the lower (i.e. fluid–fluid) interface and thus moving faster than the bottom layer when departing from the lip. This then would lead to thinning at an accelerated rate compared to a single layer and may cause break-up at a higher flow rate than for a purely single layer of fluid.

Fig. 8 shows the equivalent data for a 3-layer curtain, with the same fluid as in Figs. 6 and 7. In Fig. 8(a) and (b), the variable parameters were Q_3 and Q_2, respectively as per the procedure described in Section 2.2. Note that the number of data points is necessarily reduced due to the operational low-flow rate limits of the pumps. Here, $Q_{T,min}$ is in good agreement with that found from the 1-layer experiment and again that the true hysteresis window has been significantly reduced. However, there is a difference between the hysteresis windows in Fig. 8(a) and (b); in Fig. 8(a), when Q_3 was varied, the true hysteresis window is small and there is a large range in the data for $Q_{T,thr}$ whereas in Fig. 8(b), when Q_2 was varied, the true hysteresis window is larger than the range of $Q_{T,thr}$.

For a slightly more viscous curtain with $\mu_{1,2,3} = 33.4$ mPa s, it is again observed that $Q_{T,min} \approx Q_{min}$ but a reduced true hysteresis window, shown in Fig. 9(a). However, for a 3-layer curtain, shown

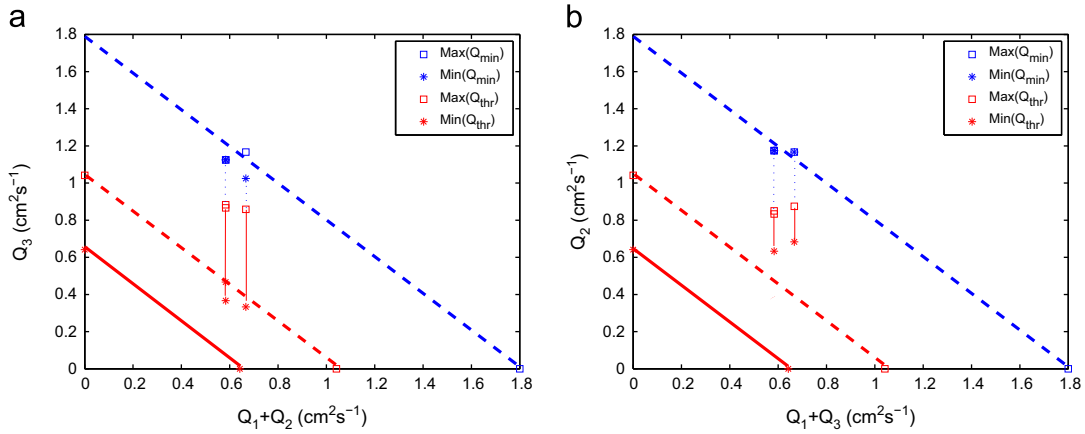

Fig. 8. Plot of Q_{min} and Q_{thr} for a 3-layer curtain where all layers are the same fluid ($\mu=15.4$ mPa s, $\rho=1171$ kg/m^3, $\sigma=47.9$ mN/m). In (a) Q_3 was varied whilst in (b) Q_2 was varied. The diagonal dashed lines plot the "expected" limits of the hysteresis window based on the 1-layer experiments in Fig. 6.

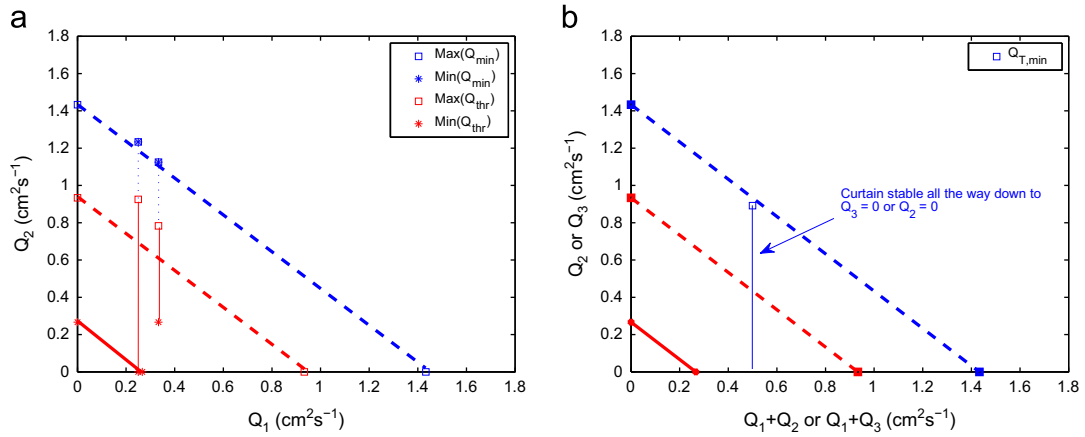

Fig. 9. Plot of Q_{min} and Q_{thr} for (a) 2-layer and (b) 3-layer curtain where all layers are the same fluid ($\mu=33.4$ mPa.s, $\rho=1196$ kg/m^3, $\sigma=42.2$ mN/m). In (b) no break-up was observed for either experiment (i.e. where Q_2 or Q_3 was varied). The diagonal dashed lines plot the "expected" limits of the hysteresis window based on the 1-layer experiments for the same fluid.

in Fig. 9(b), the curtain always remains stable for the range of flow rates that are feasible with the current experimental setup, since the combined flow rate of two layers, each at the minimum possible flow rate, is approximately 0.5 cm^2 s^{-1}, which was stable for all realisations herein.

Thus, in summary for the low-viscosity multi-layer Newtonian curtains, it is seen that $Q_{T,min} \approx Q_{min}$, but the true hysteresis window is small compared to the single layer curtain.

4.3. Multiple layers of different fluids

Fig. 10 shows data from experiments with 2-layer curtains composed of different fluids. In Fig. 10(a), both layers are of the same viscosity, but the surfactant concentration is different. When the lower surfactant concentration fluid was used as the bottom layer (Q_1), it is found that $Q_{T,min}$ agrees exactly with Q_{min} found in the 1-layer experiment, but a slightly extended hysteresis window. In contrast, when the higher surfactant fluid is used as Q_1, it is found that $Q_{T,min} > Q_{min}$ and a considerably larger hysteresis window. Note that in Fig. 10(a), the diagonal lines indicate data from the 1-layer experiments with the *higher* surfactant fluid (i.e. $\sigma = 42.2$ mN/m).

In Fig. 10(b) and (c), the same low-σ fluid from (a) was used in combination with higher viscosity fluids with $\mu=86$ and 296 mPa s respectively. The surfactant concentration was matched in both cases. Here, the 2-layer data is in good agreement with the 1-layer data, where the 1-layer data plotted in both (a) and (b) is for the more viscous fluid. The only notable difference is the slightly extended hysteresis window in Fig. 10(c) where the low-viscosity fluid was used for Q_1. Otherwise, it appears that when surfactant concentrations are matched, viscous effects dominate and the 2-layer curtain composed of a high and low-viscosity fluid behaves in a similar fashion to the 1-layer high-viscosity curtain. This observation supports the choice of μ_1 in the formation of the dimensionless groups, such as the Reynolds number.

4.4. Normalised hysteresis windows

The hysteresis windows obtained for 1-layer and 2-layer curtains using the experimental procedure outlined in the above sections can be quantitatively compared by plotting the window for 2 layers against the window for 1-layer curtains, as shown in Fig. 11. Here, the absolute size of the window, $\min(Q_{min}) - \max(Q_{thr})$ in cm^2 s^{-1}, is plotted and it is seen that the window is only extended for 2-layer curtains when angled edge guides are employed, shown by the triangle data points residing above the dashed line. Even in these isolated cases, the window is not appreciably extended and all other data lie below the dashed line, indicating that in general, the hysteresis window is wider for the 1-layer curtains.

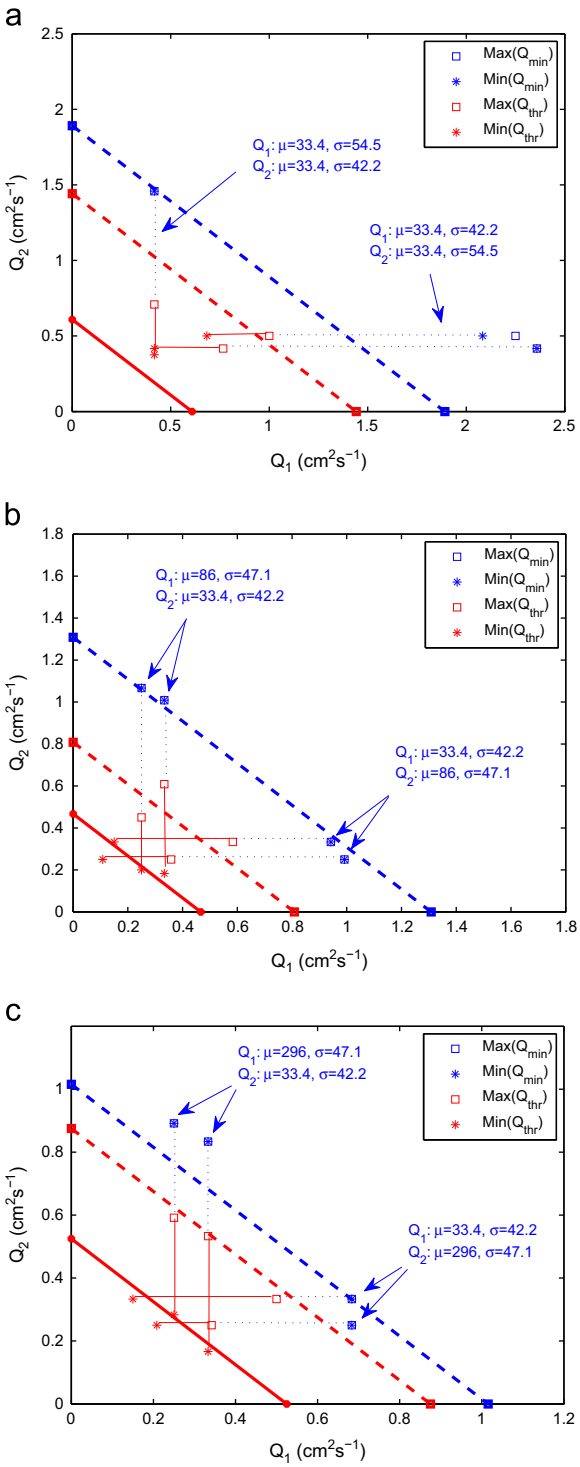

Fig. 10. Plot of Q_{min} and Q_{thr} for 2-layer curtains with (a) $\mu=33.4$, $\sigma=42.4$ and $\mu=33.4$, $\sigma=54.5$; (b) $\mu=86$, $\sigma=47.1$ and $\mu=33.4$, $\sigma=42.2$; and (c) $\mu=296$, $\sigma=47.1$ and $\mu=33.4$, $\sigma=42.2$. In each case, both fluids were used as Q_1 and Q_2 as indicated by the arrows in the plots. The diagonal lines plot the "expected" limits of the hysteresis window based on the 1-layer experiments for the most viscous fluid in each plot.

Using the raw data for the hysteresis windows, one can also define a *normalised* hysteresis window as

$$Q_{norm} = \frac{Q_{T,min} - Q_{T,thr}}{Q_{min}}. \tag{17}$$

Using this definition, the hysteresis is shown as a function of the number of layers for two low-viscosity fluids in Fig. 12. Here,

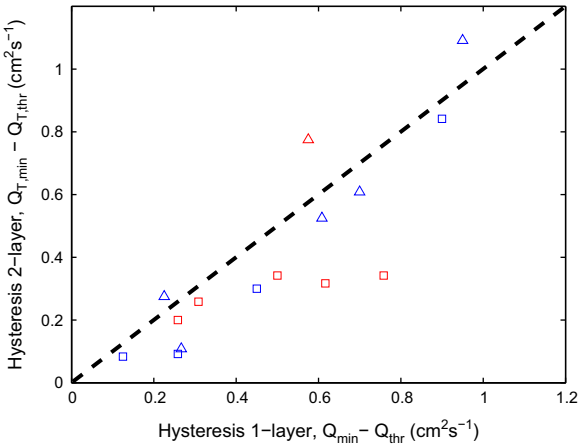

Fig. 11. Hysteresis windows for 1- and 2-layer curtains of the same fluid. Red data points indicate surfactant solutions, whilst triangles indicate angled edge guides. The dashed line corresponds to parity. (For interpretation of the references to colour in this figure caption, the reader is referred to the web version of this paper.)

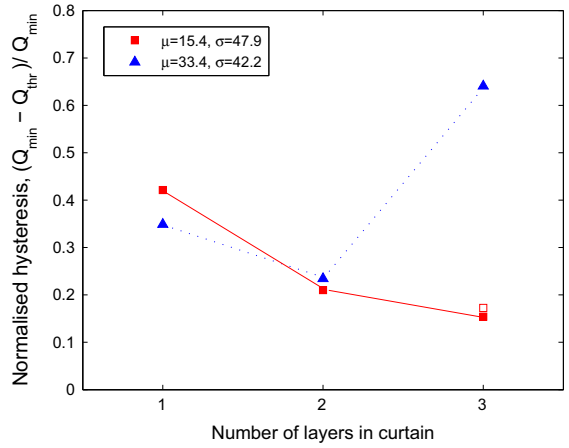

Fig. 12. Normalised hysteresis window versus number of layers where each layer is the same fluid, $\mu=15.4$ mPa s, $\rho=1171$ kg/m^3, $\sigma=47.9$ mN/m. The red data point for 3 layers is where Q_2 was varied instead of Q_3. (For interpretation of the references to colour in this figure caption, the reader is referred to the web version of this paper.)

for the $\mu=15.4$ mPa s fluid, the data are in accord with those found in Fig. 11, with decreasing windows for both 2 layers and 3 layers. However, there is a dramatic increase in the window size for the 3-layer curtain with $\mu=33.4$ mPa s. Physically, this result corresponds to the situation where a large flow rate is required in the top layer to form a stable curtain, but the flow rate could then be reduced to zero before the curtain ruptures, thus yielding a large hysteresis window.

In Fig. 13, the influence of viscosity is isolated by considering only the fluids without surfactant, namely PVA and higher-viscosity glycerol solutions. Data for both the straight and angled edge guides have been plotted. The largest hysteresis window occurs for the lowest viscosity (i.e the PVA solution), which then reduces to a minimum window size of approximately 0.1 at $\mu=123$ mPa s, after which the window then increases again as the viscosity increases. This trend is mirrored by the data for the angled edge guides.

4.5. Summary of hysteresis observations

The data presented in this section shows that the hysteresis window in curtain stability can be significant, but that it may be

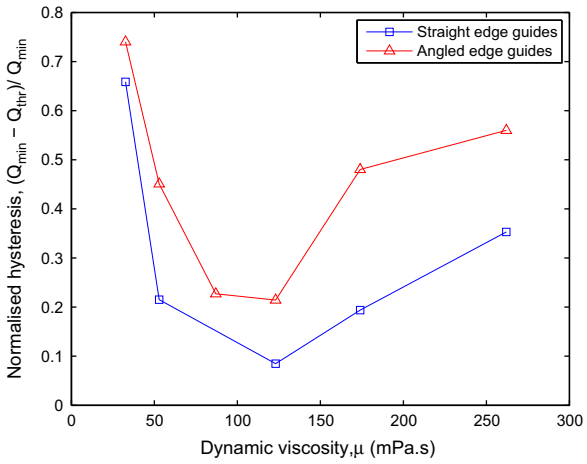

Fig. 13. Normalised hysteresis window versus viscosity for 1-layer curtains of liquids without surfactant.

reduced when using multiple layers composed of the same or different fluids. When the curtain is composed of multiple layers of the same fluid, the layers are separated only by the differential motion between them, and possibly bulk surfactant concentration differences, since the top face and the rear face of the curtain are exposed to the ambient. As such, there appears to be a confluence of interfacial tension due to surfactant migration and velocity gradients. Certainly a top layer subject to free-slip at the lower boundary may induce a modified velocity distribution compared to a single layer. Coupled with the complex fluid interaction close to the edge guides (see Section 6 below), this may partly explain some of the observed phenomena here.

5. Break-up origins

Analysis of high-speed video data allows us to determine with reasonable accuracy ($\pm$ 1 mm) the location of the origin of the break-up of the curtain. Fig. 14 shows data from 142 realisations, for both 1-layer and 2-layer experiments using both straight and angled edge guides. The legend in the right side indicates the viscosity and the surface tension of each layer. In general, it appears that most break-ups originate from within 2–3 cm of the straight edge guides, whilst the break-up origins for the angled edge guides are much more evenly distributed across the width of the curtain. This is more readily seen in Fig. 15, where all available experimental data from the video sequences is included. As seen, there is a clear bias towards the edge regions for the straight edge guides, with a notable number occurring within 1 cm of the edge guide, which coincides with the possible boundary layer thickness calculated from Eq. (14).

The observation of break-up occurring predominantly in the edge regions for straight guides and near the centre for tapered guides has been explained by Miyamoto and Katagiri (1997) by considering the flow close the edge guides themselves as follows: for vertical edge guides, the inherent development of a boundary layer induces lateral flow, directed towards the centre of the curtain. This creates a local thinning near the edge guides which, in addition to the slower flow, leaves it more prone to break-up than the central region. Conversely, the edge guide wettability also comes into play since a highly wettable surface will induce a capillary force drawing liquid toward the edge region. This then acts to thicken the film in the vicinity of the edge guide. Thus there is competition between these two effects, both of which are clearly dependent on the physical properties of the liquid being used. All else being equal, however, a tapered edge guide, i.e. one which is

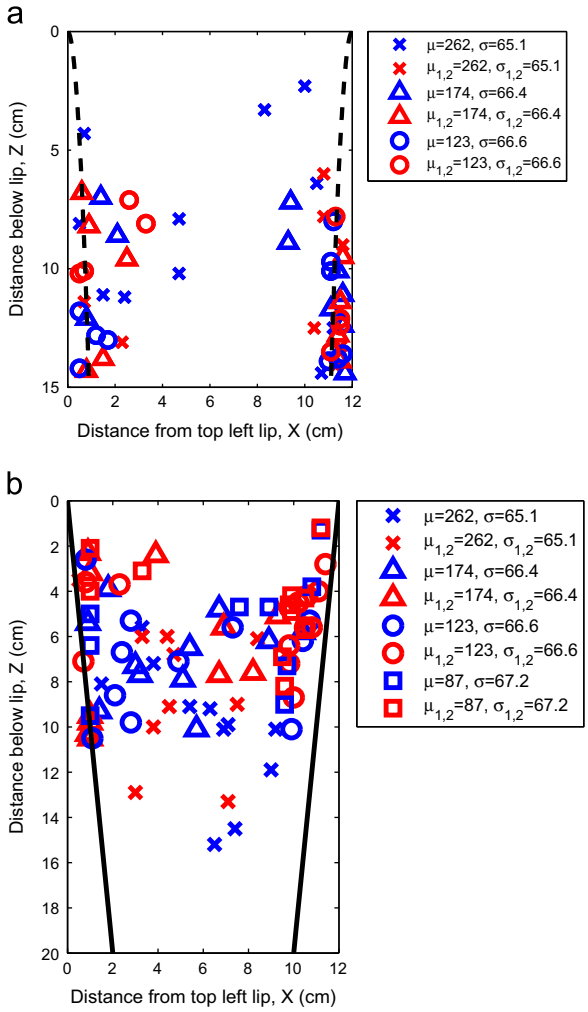

Fig. 14. Plot of the origins of curtain break-up for 1-layer (blue) and 2-layer (red) for (a) straight edge guides and (b) angled edge guides. A total of 142 realisations are plotted here. The dashed black lines in (a) indicate the extent of boundary layer effects based on (14) and (15), whilst the solid black lines in (b) indicate the surface of the angled edge guides. (For interpretation of the references to colour in this figure caption, the reader is referred to the web version of this paper.)

inclined from vertical so that the base of the curtain is narrower than the top, will act to counter the inherent thinning in the curtain due to acceleration and boundary layer effects, thus increasing the stability compared to a straight, vertical edge guide. This effect will be more pronounced in the edge regions where the boundary layer develops. In contrast, the central region of the curtain is likely to be less affected by this as it will continue to accelerate uniformly under gravity. Thus the curtain is expected to break-up from the central regions, where the curtain is at its thinnest, for any given height. The effect of edge guide wettability was also highlighted by Kistler and Scriven (1994).

5.1. Rupture speed

Fig. 16 shows an image sequence from a high-speed video of the opening and the closing of a hole at the base of the curtain. The hole is initiated due to a disturbance which punctures the free-surface at approximately 10 cm below the lip of the die. At this height, the curtain velocity $v_c \approx 1.5$ m/s, indicating that the local curtain thickness $h_c = Q/v_c \approx 45$ μm. The hole opens downward in the vertical direction, but never exceeds the initial vertical location, that is to say the disturbance does not propagate upstream. Note that for this realisation, $We > 1$.

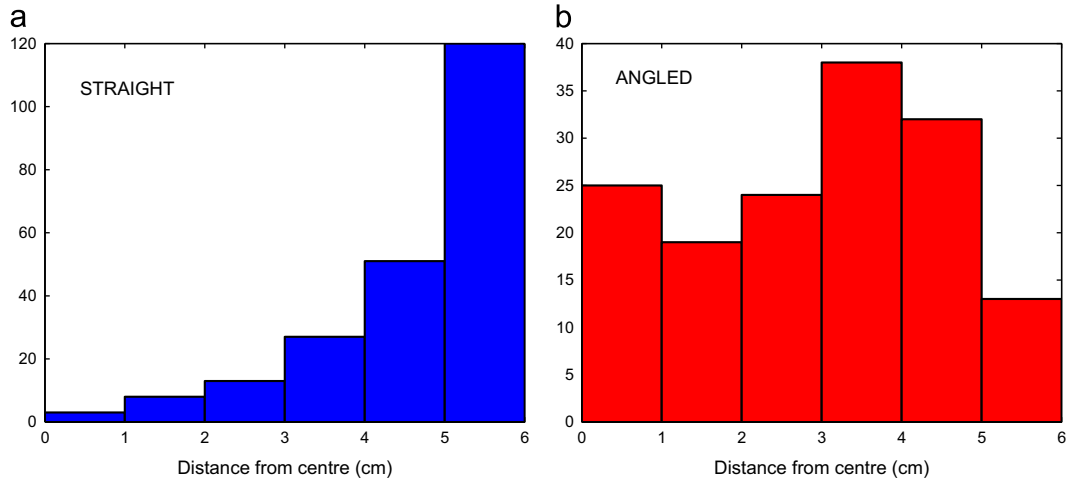

Fig. 15. Plot of break-up origins measured from the centre of the curtain for (a) straight and (b) angled edge guides. The total frequency incorporates 1-, 2- and 3-layer data for all fluids used herein, corresponding to a total of 372 experimental data points.

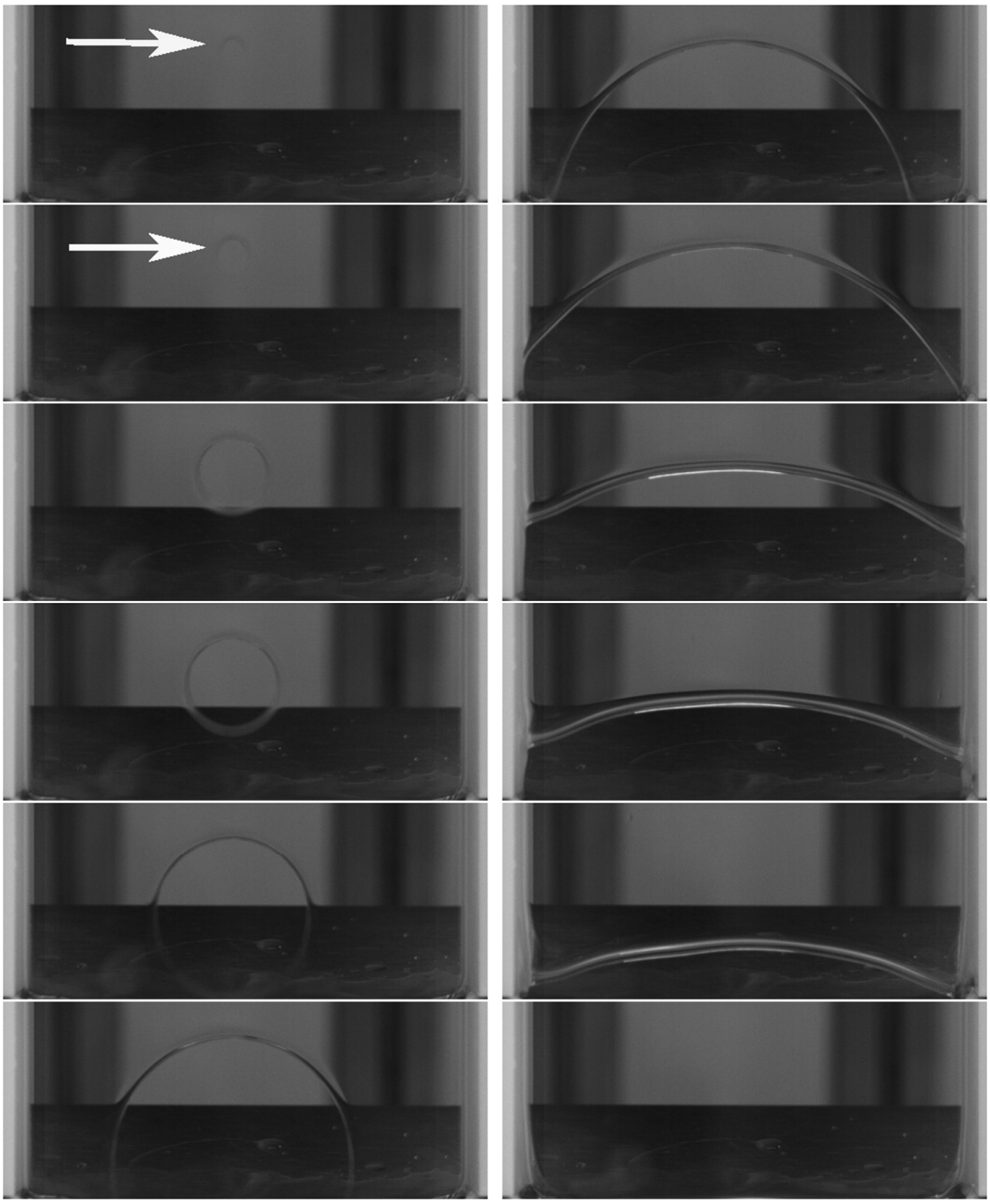

Fig. 16. Snapshots from a high-speed video sequence showing the puncture (left panel) and then re-forming of a stable curtain (right panel). The arrows in the first two images indicate the hole in its early stages. Taking the first image as the reference frame, subsequent frames are taken at $t=1$, 3, 7, 13, 21, 33, 49, 97, 137, 177 and 217 ms. $\mu=262$ mPa s, $Re=0.32$, $We=1.15$.

By measuring the hole radius versus time from initial rupture, one can determine the speed of rupture for various cases. In Fig. 17, two such examples are presented for both a 90% and a 80% glycerol–water mixture, both containing surfactant. In each realisation, both the vertical and the horizontal extent of the hole are shown, but there is no discernible difference between the two. The dashed lines indicate best fits to the data, thus exhibiting constant opening speeds of 1.39 and 1.25 m/s, respectively for the 90% and 80% solutions (μ=281 and 70 mPa s). By calculating the local curtain speed at the point of initial rupture, the local thickness in these realisations is estimated to be $h_c = 45$ and 61 μm. By using the measured physical properties, one can then determine the predicted opening speeds from the Taylor–Culick velocity, Eq. (5), which for these examples are 1.43 and 1.12 m/s, respectively. These show very good agreement with the measured velocities, which indicates that the effective surface tension of the curtain at the point of rupture is indeed close to the equilibrium value, as measured by the static values given in Table 1.

A full assessment of the opening speeds for various realisations is shown in Fig. 18, where the experimentally determined opening speed is plotted against the Taylor–Culick speed for curtain break-ups occurring across a range of physical properties. The solid line indicates parity between the two. In general, the experimental velocities are marginally lower than the predicted speed, which may be due to error in estimating the local curtain thickness as well as viscous effects. Nonetheless, it appears that for this process, where surfactants are used, the use of an equilibrium value of surface tension in the curtain (once several centimetres away from the lip) is justified. This, of course, is not likely to be the case for the flow along the face of the die or near the lip region.

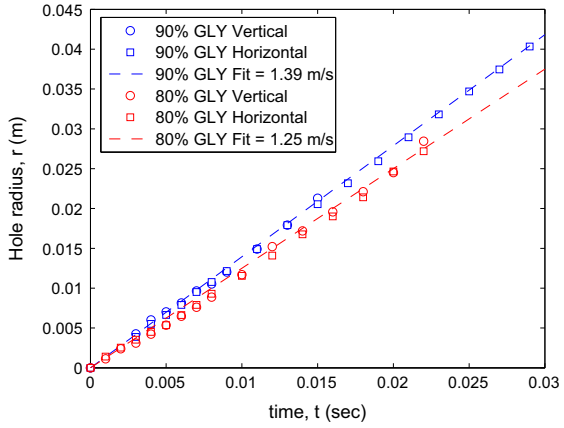

Fig. 17. Hole radius versus time from moment of rupture for two glycerol–water mixtures with surfactant. Data for both the horizontal and vertical extents are shown, with negligible difference in these opening stages. The dashed lines correspond to linear best fits, both with correlation coefficients $R^2 = 0.997$.

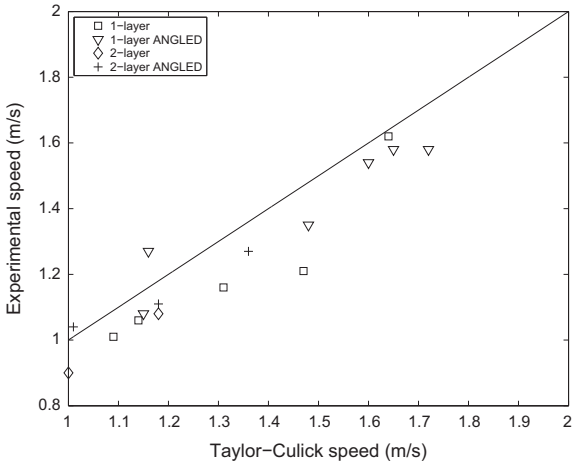

Fig. 18. Measured hole opening speeds versus the predicted Taylor–Culick speed for different realisations, encompassing a range of viscosities from μ=70 to 281 mPa s. The solid line indicates parity.

6. Weber number criterion

In order to quantitatively assess the Weber number criteria of Brown (1961) and Dyson et al. (2009) for 1-layer and multi-layer curtains respectively, one must first locate the vertical origin, z, of the disturbance that ultimately breaks the curtain (as in Fig. 15, see previous section). This location is then used to calculate the local curtain velocity, $v_c = (2gz)^{1/2}$, and in turn, the local Weber number, where for a 1-layer curtain we use Eq. (1) and for a 2- or 3-layer curtain we use Eq. (16). When angled edge guides are used, we also compensate for the change in flow rate per unit width using Eq. (6).

Figs. 19 and 20 plot the critical Weber number evaluated at break-up versus viscosity and surface tension, respectively. In Fig. 19, a peak

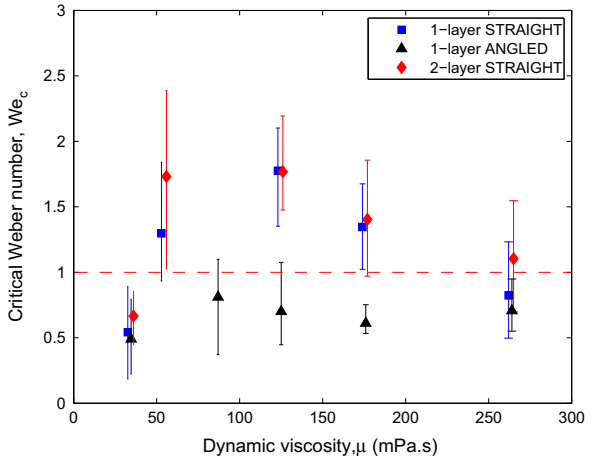

Fig. 19. Critical Weber number evaluated at the break-up origin for both straight and angled edge guides and 2-layer curtains. The viscosity values for black and red symbols have been offset by +2 mPa s for visualisation purposes only. The red dashed line indicates We=1. (For interpretation of the references to colour in this figure caption, the reader is referred to the web version of this paper.)

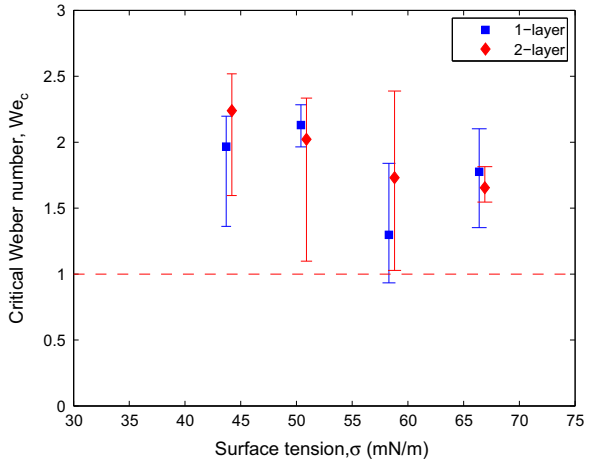

Fig. 20. Critical Weber number evaluated at the break-up origin for both 1-layer and 2-layer curtains of the same fluid (glycerol–water solutions with various levels of surfactant) with straight edge guides. The surface tension values for red symbols have been offset by +0.5 mN/m for visualisation only. (For interpretation of the references to colour in this figure caption, the reader is referred to the web version of this paper.)

critical Weber number occurs at $\mu \approx 130$ mPa s, which drops off either side as the viscosity is increased or decreased. Note that this "peak" phenomenon is robust as it is also observed for both the 2-layer and 1-layer curtains. This also corresponds to the viscosity at which the minimum hysteresis was found (see Fig. 13). The most striking observation here is that the use of angled edge guides almost always leads to critical Weber numbers less than unity, i.e. $We_c < 1$, which is more readily seen for the mid-range viscosities. The lowest and highest viscosities in this figure (for PVA and 90% glycerol solution respectively) form remarkably stable curtains even for the straight edge guides so that the difference between the straight and angled data sets is significantly diminished.

In Fig. 20, good agreement is again found between 1-layer and 2-layer data sets, but no quantifiable trend in terms of surface tension. All the fluids in this plot were glycerol-based solution of similar viscosity with added surfactant.

For both Figs. 19 and 20, the critical Weber numbers for both the 1-layer and 2-layer curtains largely coincide, which certainly supports the use of Eq. (16) derived by Dyson et al. (2009) for multi-layer curtains. To our knowledge, this represents the first systematic experimental validation of this equation.

Finally, Fig. 21 plots all data obtained in this experimental study in the form of curtain inertia, $v_c \sum(\rho_i Q_i)$, versus total surface tension, $\sum\sigma_i$. Note that for clarity, only the mean values (without error bars) have been plotted. The solid black line indicates a slope of 1, i.e. where $We = 1$, showing that only a few experimental conditions violated this

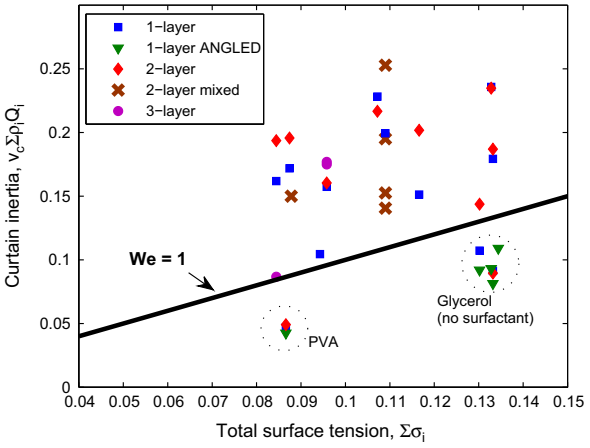

Fig. 21. Curtain inertia at the onset of break-up versus total surface tension for all fluids tested in this study. The data points represent the mean values from each data set. The solid black line represents a slope of 1, i.e. where $We = 1$.

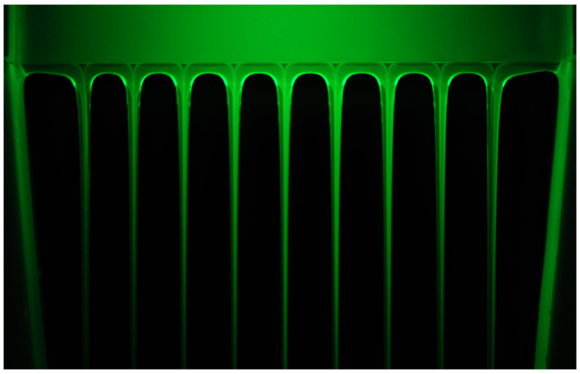

Fig. 22. Fluorescence imaging of the thread structure after break-up of a 3-layer curtain. Fluorescein dye is in the middle layer with a flow rate of $Q_2 = 0.22$ cm^2 s^{-1}, whilst the flow rate in both the top and bottom layers is $Q_1 = Q_3 = 0.63$ cm^2 s^{-1}. The total image width is 12 cm.

well-established stability criterion. In particular, note that only the polymer-based PVA solution and the most viscous glycerol-based solutions (without surfactant) violate the criterion for straight 1-layer and 2-layer curtains, but that all the curtains using angled edge guides also violate this criterion. None of the 2-layer or 3-layer curtains containing surfactant, whether composed of the same or different fluids, were found to violate the $We > 1$ condition. Note that attempting to collapse data in terms of the *surface pressure* did not reveal any trend, such as that found by De Luca and Meola (1995), presumably due to the relatively narrow range of surface tensions but broad range of viscosities in our study, in contrast to their relatively broad range of surface tensions with the narrow viscosity range.

7. Thread structure after break-up

In addition to high-speed video sequences of the overall break-up process, fluorescence imaging was used to study the thread structure after break-up. Here, a qualitative overview of observations of the structure of threads composed of multiple layers is given, in addition to measurements of the thread spacing.

7.1. Qualitative features

Fig. 22 shows an image of the full curtain width after break-up of a 3-layer curtain, where fluorescein is present in the middle layer. In addition, Fig. 23 shows a close-up of the lip region for very similar flow rates. Both figures exhibit an interesting observation, namely the dark triangular patches located directly below the lip of the die at the centre-line of the threads. This indicates that there is a localised "squeezing" of the middle layer at this point.

Furthermore, Fig. 24 presents images of a 2-layer thread, which shows the progressive encapsulation of the bottom layer as the flow rate in the top layer is increased. Note that fluorescein is present in the bottom layer only. The bottom layer becomes pinned at the back of the lip and the top layer flows over and around the thread from the bottom layer to form an encapsulated or "compound" thread structure.

7.2. Quantitative assessment of spacing

Fig. 25(a) shows the absolute values of the thread spacing versus total flow rate, and Fig. 25(b) shows the normalised spacing versus Weber number. From Fig. 25(a), it is clear that the thread spacing is independent of the flow rate, a conclusion also made by Giorgiutti et al. (1995) for threads formed from silicone oils emanating from a cylinder. It is observed that the thread spacing for all flow rates varies between 1.1 and 1.4 cm, which is also smaller than the lengthscale from the Rayleigh–Taylor instability

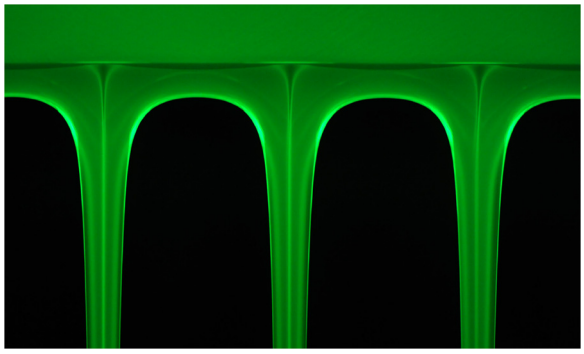

Fig. 23. Close-up of the thread structure after the break-up of a 3-layer curtain with fluorescein in the middle layer. Flow rates are $Q_1 = Q_3 = 0.55$ cm^2 s^{-1} and $Q_2 = 0.2$ cm^2 s^{-1}. The total image width is 3.5 cm.

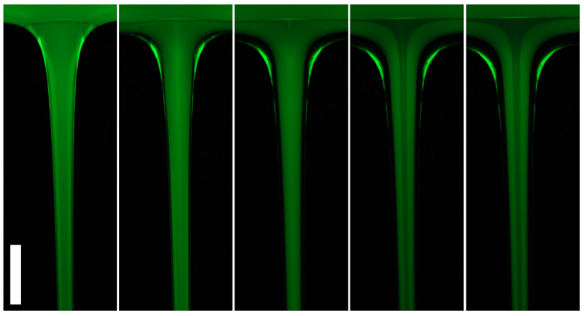

Fig. 24. Fluorescence imaging of the thread structure after break-up of a 2-layer curtain. In all cases fluorescein dye is in the bottom layer with a fixed flow rate of Q=0.2 cm^2 s^{-1}, whilst the flow rate in the top layer increases from right to left with Q=0.5, 0.67, 1.0, 1.23 and 1.35 cm^2 s^{-1}. The scale bar is 5 mm.

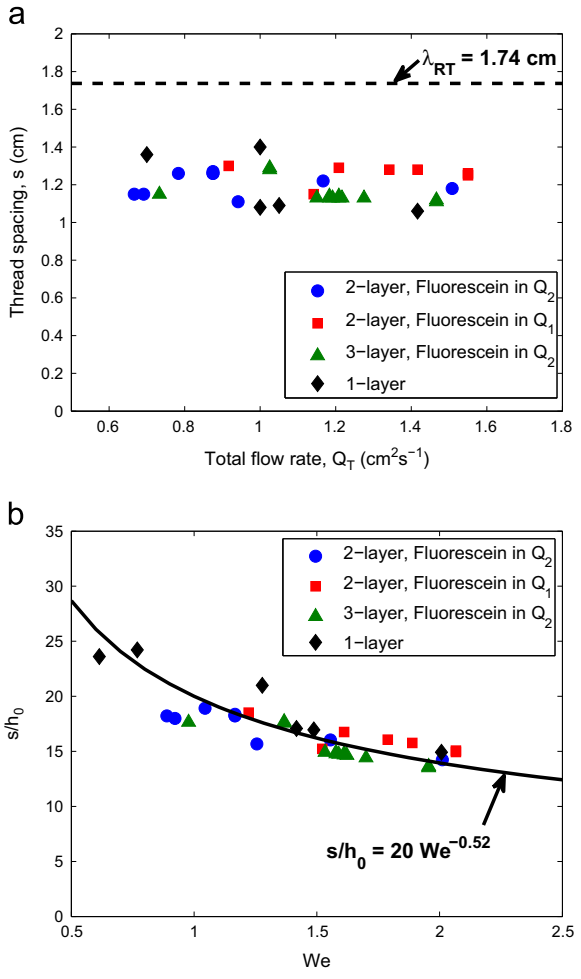

Fig. 25. Thread spacings for 2- and 3-layer curtains after break-up. (a) shows the raw measurement plotted as a function of total curtain flow rate, whilst (b) shows the normalised spacing versus Weber number. The dashed line in (a) corresponds to the lengthscale, $\lambda_{RT}=1.74$ cm, from the Rayleigh–Taylor instability and the solid line in (b) plots the empirical equation $s/h_0=20We^{-0.52}$ from De Luca and Meola (1995).

corresponding to the most unstable mode (Limat et al., 1992), which for this fluid corresponds to $\lambda_{RT}=2\pi\sqrt{2\sigma/(\rho g)}=1.74$ cm. Note that in Fig. 25(a), data is shown for 2-layer curtains where the order of the layers was reversed and 3-layer curtains, but there is no distinguishable trend between the respective data sets. The 1-layer data points were from different glycerol solutions without fluorescein, so the lengthscale $\lambda_{RT}=1.74$ cm does not apply to those.

In Fig. 25(b), the same data from 25(a) is plotted but the spacing has been normalised by h_0, which corresponds to the approximate film thickness before departing from the lip. In De Luca and Meola (1995), h_0 was taken precisely as the slot exit width. However, for the current experimental setup one must use an approximation $h_0=Q_T/v_0$, where v_0 is the speed of the liquid film just prior to departing the lip, which is calculated using Eq. (15). The flow rate has also been non-dimensionalised in the form of the Weber number. Under these scalings, the data collapses reasonably well and can be adequately described by the original empirical Eq. (3) from de Luca and Meola.

Of course, in the absence of direct measurements of v_0 for each individual realisation, the agreement between the present experimental data and the equation given depends on the approximation used for h_0 and, by extension, v_0. However, given that the range of values for $v_0=0.11$–0.17 m/s calculated by (15) are in good quantitative agreement with measured values of around 0.13 m/s, the choice of this approximation can be justified. Since the experimental setup herein employs a slide die and that of de Luca and Meola employed a slot die, it thus appears that the spacing of the threads formed after break-up is insensitive to both the number of layers in the curtain *and* the exit geometry of the curtain.

8. Conclusions

In conclusion, an experimental investigation of the formation and break-up of liquid curtains comprising 1, 2 and 3 layers has been performed. Both the flow rate at which a stable curtain could be formed, $Q_{T,min}$, and the reduced flow rate at which the curtain becomes unstable, $Q_{T,thr}$, were assessed. The difference between these two flow rates defines a hysteresis window. In general, it was found that the hysteresis window for 2- and 3-layer curtains was reduced from that found with a single layer. In general, $Q_{T,min}$ for multiple layers was in good agreement with Q_{min} for 1-layer curtains. However, $Q_{T,thr}$ was found to vary considerably from the 1-layer experiments. For 3-layer curtains, the hysteresis window was also dependent upon which flow rate was chosen as the variable parameter (i.e. whether Q_2 or Q_3 was varied). It was proposed that the differential motion between the layers in the initial stages and the migration of surfactant to the interfaces yields a complex dynamical situation, which may be the cause of the observed hysteresis and certainly warrants further examination using numerical tools.

The origin of the break-up, determined from high-speed video, was found to be strongly dependent on the edge guides used (i.e. straight vs. angled), whereby the break-up origin from straight edge guides was normally confined to within 2 cm from the edge, whereas no such trend was observed with the angled edge guides. Using the exact location, the local Weber number at the moment of break-up was calculated and was found to be dependent on both the liquid viscosity and the edge guides. The Weber number criteria of Brown (1961) and Dyson et al. (2009) were tested and it was found that for straight curtains, there is a viscosity dependence, which was absent for tapered curtains. However, the critical Weber number was rather insensitive to surface tension. In summary, apart from the tapered curtain geometry, only the high-viscosity glycerol solutions *without* surfactant and the polymer-base PVA solutions violated the Weber number criterion.

In addition to the observations of break-up, fluorescence imaging of the threads formed after the rupture of multi-layer curtains revealed some interesting features, such as localised “squeezing” of the middle layer directly below the lip of the die for 3 layers and thread encapsulation for 2 layers. The thread spacing was assessed and found to be smaller than the wavelength predicted from the Rayleigh–Taylor instability, however, was well-described using a previously developed empirical relationship from De Luca and Meola (1995).

This report constitutes, to the author's knowledge, the first systematic investigation of the flow-rate hysteresis in curtain stability and the first experimental validation of the Weber number criteria for multi-layer curtains. Ongoing extensions to this work include experimental verification of the stability criteria for non-Newtonian fluids and modelling of the curtain stability under the combined influence of surfactants and complex non-Newtonian rheologies.

Acknowledgments

This work was partially supported by an Academic Excellence Alliance grant awarded by the KAUST office of Competitive Research Funds number 7000000028. The experimental work was conducted while J.T. and D.H. were on research visits at KAUST. We thank the Analytical Core Laboratory and Sahraoui Chaieb at KAUST for assistance with characterisation of the fluid physical properties. We also thank Thomas Ramel and Maick Nielsen from TSE Troller AG for technical advice and guidance for certain aspects of the experimental work.

References

Antoniades, M.G., Godwin, R., Lin, S.P., 1980. A new method of measuring dynamic surface tension. J. Colloid Interface Sci. 77, 583–585.
Becerra, M., Carvalho, M.S., 2011. Stability of viscoelastic liquid curtain. Chem. Eng. Proc. 50, 445–449.
Bird, R.B., Stewart, W.E., Lightfoot, E.N., 2007. Transport Phenomena, second edition, John Wiley & Sons, New York.
Blake, T.D., Clarke, A., Ruschak, K.J., 1994. Hydrodynamic assist of dynamic wetting. AIChE J. 40, 229–242.
Blake, T.D., Dobson, R.A., Ruschak, K.J., 2004. Wetting at high capillary numbers. J. Colloid Interface Sci. 279, 198–205.
Brenner M.P., Gueyffier D., On the bursting of viscous sheets. Phys Fluids 11, 1999, 737-739.
Brown, D.R., 1961. A study of the behaviour of a thin sheet of moving liquid. J. Fluid Mech. 10, 297–305.
Brunet, P., 2007. Pattern-forming instabilities: a phenomenological approach through simple examples. Eur. J. Phys 28, 215–230.
Brunet, P., Flesselles, J.M., Limat, L., 2007. Dynamics of a circular arrays of liquid columns. Eur. Phys. J. B 55, 297–322.
Clarke, A., Weinstein, S.J., Moon, A.G., Simister, E.A., 1997. Time-dependent equations governing the shape of a two-dimensional liquid curtain, Part 2: experiment. Phys. Fluids 9, 3637–3644.
Doell, H., Gerlach, D., Alleborn, N., Delgado, A., 2009. Influence of rheology and geometry on the teapot effect of a curtain coater. Eur. Phys. J 166, 133–137.
Dyson, R.J., Brander, J., Breward, C.J.W., Howell, P.D., 2009. Long-wavelength stability of an unsupported multilayer liquid film falling under gravity. J. Eng. Math. 64, 237–250.
Finnicum, D.S., Weinstein, S.J., Ruschak, K.J., 1993. The effect of applied pressure on the shape of a two-dimensional liquid curtain falling under the influence of gravity. J. Fluid Mech. 255, 647–665.
Giorgiutti, F., Bleton, A., Limat, L., Wesfreid, J.E., 1995. Dynamics of a one-dimensional array of liquid columns. Phys. Rev. Lett. 74, 538–541.
Jiang, W.Y., Helenbrook, B.T., Lin, S.P., Weinstein, S.J., 2005. Low-Reynolds-number instabilities in three-layer flow down an inclined wall. J. Fluid Mech. 539, 387–416.
Kistler, S.F., Scriven, L.E., 1994. The teapot effect: sheet-forming flows with deflection, wetting and hysteresis. J. Fluid Mech. 263, 19–62.
Limat, L., Jenffer, P., Dagens, B., Touron, E., Fermigier, M., Wesfried, J.E., 1992. Gravitational instabilities of thin liquid layers: dynamics of pattern selection. Physica D 61, 166–182.
Lin, S.P., Krishna, V.G., 1978. Deflection of a viscous liquid curtain. Phys. Fluids 21 (12), 2367–2368.
Lin, S.P., Roberts, G., 1981. Waves in a viscous liquid curtain. J. Fluid Mech. 112, 443–458.
Lin, S.P., 1981. Stability of a viscous liquid curtain. J. Fluid Mech. 104, 111–118.
Lin, S.P., Lian, Z.W., Creighton, B.J., 1990. Absolute and convective instability of a liquid sheet. J. Fluid Mech. 220, 673–689.
De Luca, L., Meola, C., 1995. Surfactant effects on the dynamics of a thin liquid sheet. J. Fluid Mech. 300, 71–85.
De Luca, L., Costa, M., 1997. Instability of a spatially developing liquid sheet. J. Fluid Mech. 331, 127–144.
De Luca, L., 1999. Experimental investigation of the global instability of plane sheet flows. J. Fluid Mech. 399, 355–376.
Marston, J.O., Simmons, M.J.H., Decent, S.P., Kirk, S.P., 2006. Influence of the flow field in curtain coating onto pre-wet substrates. Phys. Fluids.
Marston, J.O., Simmons, M.J.H., Decent, S.P., 2007. Influence of viscosity and impingement speed on intense hydrodynamic assist in curtain coating. Exp. Fluids 42, 483–488.
Miyamoto, K., Katagiri, Y., 1997. Curtain coating. In: Kistler, S., Schweizer (Eds.), Liquid Film Coating. Chapman-Hall, London, pp. 463–494.
Pritchard, W.G., 1986. Instability and chaotic behaviour in a free-surface flow. J. Fluid Mech. 165, 1–60.
Roche, J.S., Le Grand, N., Brunet, P., Lebon, L., Limat, L., 2006. Perturbations on a liquid curtain near break-up: wakes and free edges. Phys. Fluids 18, 082101.
Savva, N., Bush, J.W.M., 2009. Viscous sheet retraction. J. Fluid Mech. 626, 211–240.
Schweizer, P.M., Troller, U., 2000. Method and Apparatus for Curtain Coating Providing a Lateral Liquid Film Velocity Equal to the Curtain Falling Velocity. US Patent 6,048,582.
Schweizer, P., Krebs, F., 2003. Liquid Film Coating Process. US Patent 0235657A1.
Sunderhauf, G., Raszillier, H., Durst, F., 2002. The retraction of the edge of a planar liquid sheet. Phys. Fluids 14, 198–208.
Taylor, G.I., 1959. The dynamics of thin sheets of fluid. III. Disintegration of fluid sheets. Proc. R. Soc. Lond. A 253, 313–321.
Weinstein, S.J., 1990. Wave propagation in the flow of shear-thinning fluids down an incline. AIChE J. 36, 1873–1889.
Weinstein, S.J., Clarke, A., Moon, A.G., Simister, E.A., 1997. Time-dependent equations governing the shape of a two-dimensional liquid curtain, Part 1: Theory. Phys. Fluids 9, 3625–3636.
Weinstein, S.J., Hoff, J.W., Ross, D.S., 1998. Time-dependent equations governing the shape of a three-dimensional liquid curtain. Phys. Fluids 10, 1815.